Journal of Radioanalytical and Nuclear Chemistry (2021) 329:1103–1117
https://doi.org/10.1007/s10967-021-07860-3

Facile immobilization of NiFeAl-LDHs into electrospun poly(vinyl alcohol)/poly(acrylic acid) nanofibers for uranium adsorption

Jinhua Xie[1,2] · Ying Dai[1,2] · Youqun Wang[1] · Yuhui Liu[1] · Zhibin Zhang[1,2] · Yingcai Wang[1,2] · Qinqin Tao[1,2] · Yunhai Liu[1,2]

Received: 7 May 2021 / Accepted: 18 June 2021 / Published online: 26 June 2021

Abstract

Effective recovery of uranium from wastewater has positive significance to environmental treatment and the development of the nuclear industry. Through electrospinning technology, the ternary layered double hydroxide (NiFeAl-LDHs), polyvinyl alcohol (PVA) and polyacrylic acid (PAA) was used as the precursor solution to produce NiFeAl-LDHs/PVA/PAA composite nanofibers, and it can adsorb uranium under weak acid conditions. The material structure and character of the prepared fiber were analyzed by SEM, FT-IR, XRD and XPS, besides the various factors on the adsorption of uranium by the fiber under static adsorption were studied. The adsorption process of NiFeAl-LDHs/PVA/PAA to U(VI) conformed to the pseudo-second-order model ($R^2 > 0.998$). The maximum theoretical adsorption capacity of U(VI) on NiFeAl-LDHs/PVA/PAA was 203.32 mg/g at pH 6.0 calculated by the Langmuir model. The value of thermodynamic parameters showed that the adsorption process of uranium on NiFeAl-LDHs/PVA/PAA was endothermic and spontaneous. NiFeAl-LDHs/PVA/PAA can still effectively adsorb uranium after passing five adsorption–desorption cycle tests. Therefore, NiFeAl-LDHs/PVA/PAA was expected to be used in practical applications to treat uranium-containing wastewater.

Keywords Adsorption · Uranium · Electrospinning · NiFeAl-LDHs · Polyvinyl alcohol · Polyacrylic acid

Introduction

Uranium is a naturally occurring radioactive element and is the basic fuel material for the production of nuclear fuel. It generally enters environment thru mines and industry. But its chemical and radiotoxicity is of concern to human health [1]. Uranium can indirectly damage the cell membrane inhibit the respiratory chain reaction, induce the expression of apoptotic factors, and lead to cell apoptosis by affecting the normal operation of cells [2]. After being inhaled or ingested, uranium mainly affects the liver and kidneys of the human body, and can cause uremia and toxic parenchymal hepatitis in severe cases [3–5]. However, with the exploitation of uranium mining [6], utilization and post-treatment [7, 8], an increasing number of uranium-containing wastewater will be produced. The arbitrary discharge of uranium-containing wastewater would have a devastating blow to the whole biosphere of the earth [9]. The WHO have set drinking water standards for uranium in drinking water as 30 μg/L. Therefore, the effective removal of uranium in wastewater and the control of uranium mobility are of tremendous significance to protecting the environment and human health.

Adsorption [10, 11], ion exchange [12], chemical precipitation [13], electrochemistry [14] and photocatalysis [15, 16] are the most common methods to remove uranium from aqueous solution. The adsorption with low cost, high efficiency, simple operation and environmental protection is currently one of the most effective methods. At present, carbon-based materials [17, 18], titanium dioxide-based materials [19], metal–organic frameworks [20, 21], layered double hydroxide materials [22, 23], biomass materials [24, 25], and magnetic materials [26, 27] can effectively remove uranium in aqueous solutions. However, these powdered traditional

✉ Ying Dai
daiying@ecut.edu.cn

✉ Yuhui Liu
Walton_liu@163.com

[1] State Key Laboratory of Nuclear Resources and Environment, East China University of Technology, Nanchang 330013, Jiangxi, China

[2] School of Chemistry, Biological and Materials Sciences, East China University of Technology, Nanchang 330013, Jiangxi, China

adsorbents are challenging to recycle in practical applications. Electrospinning nanofibers with excellent mechanical properties can avoid the above problem perfectly [28].

Electrospinning is a technology that stretches high-molecular polymers into tiny jets under high voltage of several thousand volts, which can stably and continuously produce polymer fibers with diameters ranging from tens of nanometers to several microns. The prepared nanofiber has uniform pores, good flexibility, and was excellent supporting material. Polyacrylonitrile [29], chitosan [30, 31], cellulose [32, 33], polyvinyl alcohol [34, 35] and polyacrylic acid [36, 37] are widely used as adsorption matrix. Both PVA with hydroxyl groups and PAA with carboxyl groups have excellent hydrophilicity. The PVA and PAA can form ester group after crosslinking at 145 °C, they can not only maintain the hydrophilicity of the PVA/PAA, but also avoid the dissolution of the fiber in aqueous solutions. It has been reported to be used to adsorb Cu(II) [38], Ca(II) [39], Pb(II) [40] and other metal ions in wastewater.

Although PVA/PAA has excellent hydrophilicity and stability in aqueous media, it was low affinity and poor selectivity for uranium adsorption due to the absence of specific coordination atoms. To improve the performance of adsorbents, surface functionalization or modification of polymer, and mixing the polymer with inorganic or organic adsorbents can be used to prepare highly selective and efficient nanofiber composite adsorbents. Recently, Kim et al. [41] doped sulfhydryl-modified nano-silica nanoparticles into PVA/PAA hybrid nanofibers, while Xiao et al. [42] doped multi-walled carbon nanotubes (MWCNTs) and zero-valent iron nanoparticles (ZVI NPs), above two composite nanofiber had excellent adsorption capacity for copper (II), and reaching 125.47 and 107.8 mg/g, respectively.

Layered double hydroxides (LDHs) are metal hydroxides composed of two or more metal elements. The LDHs with unique nanostructure is simple to prepare and can selectively adsorb uranium under neutral conditions. Recently, Song et al. [43] prepared two ternary layered metal hydroxides (MgFeAl-LDHs and NiFeAl-LDHs), the maximum adsorption capacity for uranium was 188.52 and 61.16 mg/g, respectively. Meanwhile, the theoretical uranium adsorption capacity of L-cysteine intercalated Mg/al layered double hydroxides (Cys-LDHs) prepared by Wang et al. [44] was 211.58 mg/g. However, the diameters of LDHs particles are between tens to hundreds of nanometers, LDHs will be difficult to recycle and separate after adsorption. Therefore, combining the LDHs with selectively adsorbing uranium and the PVA/PAA with excellent mechanical properties will hopefully obtain an adsorbent that has the advantages of both.

In this paper, NiFeAl-LDHs was prepared and co-spun with PVA/PAA to prepare NiFeAl-LDHs/PVA/PAA, respectively. Scanning electron microscopy (SEM), Fourier transform infrared spectroscopy (FTIR), X-ray diffraction (XRD), X-ray photoelectron spectroscopy (XPS), water contact angle (WCA) and universal tensile testing machine were used to characterize the properties and structure of the nanofiber. The optimum conditions of adsorption of uranium on the two fibers were studied with different factor. The adsorption isotherm model was fitted with Langmuir, Freundlich and Duninin–Radushkevich isotherm models. The kinetic and thermodynamic values of the adsorption process were calculated, and the adsorption mechanism was discussed.

Materials and instruments

Reagents

Polyvinyl alcohol (PVA, 87 ~ 89% hydrolyzed), Polyacrylic acid (PAA, average Mw = 100,000, 35% in water), $Al(NO_3)_3{\cdot}9H_2O$, $Ni(NO_3)_2{\cdot}6H_2O$, $Fe(NO_3)_3{\cdot}9H_2O$ and urea were purchased from Sigma-Aldrich. The chemical reagents above were used directly without further purification. Deionized water was used throughout. U(VI) stock solution (1000 mg/L) was prepared in our lab [36].

Instruments

The surface appearance of NiFeAl-LDHs/PVA/PAA was observed by scanning electron microscope (SEM) (Nova NanoSEM450, FEI Corporation). The Fourier transform infrared spectroscopy (FT-IR) (Nicolet380, Thermo Nicolet Corporation) was used to identify intermolecular chemical bonds. The crystal structure of NiFeAl−LDHs sample was investigated using X-ray diffraction (XRD) (SMART preeze). The elemental composition and chemical state of the studied compounds in the research were determined by X-ray photoelectron spectroscopy (XPS). The wettability performance of the electrospinning mat surface was assessed by surveying the water contact angle. The mechanical properties were tested utilizing a universal mechanical testing machine (WDT-5, Shenzhen Kaiqiangli Experimental Instrument Company, China).

The fabrication process of materials fabrication

Preparation of LDHs and LDHs/PVA/PAA

Preparation of LDHs

NiFeAl-LDHs were prepared through hydrothermal tactics [43]. In detail a mixture of 3.0 mmol $Ni(NO_3)_2{\cdot}6H_2O$, 0.5 mmol $Al(NO_3)_3{\cdot}9H_2O$, 0.5 mmol $Fe(NO_3)_3{\cdot}9H_2O$ and 10 mmol urea was dissolved in 30 mL distilled water. Following vigorous stir for 30 min the mixture was transferred into a 50 mL Teflon lined reactor. The reactor was kept at 120 °C for 12 h. After cooling down the crude product was obtained with centrifugation, followed by washing three times with ethanol and deionized water, and drying at 60 °C for 12 h.

Preparation of LDHs/PVA/PAA using electrospinning and thermo-crosslink

The suspension of 3 wt% NiFeAl-LDHs and 10 mL H_2O was placed under ultrasonification for 30 min, followed by addition of 1.5 g PVA. The consequent mixture was magnetically stirred at 80 °C for 4 h for complete dissolution. After cooling down to room temperature 0.36 g PAA was added. The electrospinning stock solution was obtained after additional 5 h stir.

The nanofiber mat was electrospun using a horizontal electrospinning equipment (SPLab02-E, Baoding Shenchen Pump Industry Co., Ltd., China). The electrospinning parameters were set as temperature 25 °C, humidity 40%, feed rate 0.9 mL/h, the needle internal diameter 0.90 mm, the reception distance 15 cm, and the applied voltage 25 kV. The collected nanofiber converted to the final product, NiFeAl-LDHs/PVA/PAA, through heating at 150 °C for 5 h to make crosslinking reaction between PVA and PAA. The NiFeAl-LDHs free PVA/PAA used as the reference was electrospun with the similar electrospinning parameters.

Separation performance study procedure

Adsorption

The adsorption experiment was adopted to illustrate effects of various factors such as initial pH, ionic strength, initial uranium concentration, adsorption time and temperature on the adsorption performance. Prior to mixing with solid nanofibers the uranium-containing solution was treated to desired pH of 4.5–6.5 using HNO_3-NaOH solution of negligible volume and to pH of 6.5–8.0 using HNO_3-Na_2CO_3. 10 mg nanofiber (NiFeAl-LDHs/PVA/PAA or PVA/PAA) and 50 mL uranium-containing solution of specific pH were placed into a 250 mL conical flask. The uranium concentration in most experiments were controlled at 50 mg/L except the experiment of initial uranium concentration. The flask was shaken in a constant temperature water tank for a desired time, followed by solid–liquid separation through centrifugal technique. The adsorption experiment was conducted three times to increase the credibility. The uranium concentration in the solution was measured using inductively coupled plasma-optical emission spectrometry. The separation performance was assessed using the adsorption capacity (q_e, mg/g), which was calculated out using Eq. (1).

$$q_e = \frac{(C_0 - C_e)V}{m} \tag{1}$$

where C_0 (mg/L) is the initial uranium concentration, C_f (mg/L) is the final uranium concentration, V (L) is the volume of the uranium-containing solution, and m (g) is the adsorbent dosage.

Results and discussion

Characterization

The surface morphology of uranium-adsorbing and uranium free PVA/PAA and NiFeAl-LDHs/PVA/PAA were observed using SEM. The results are shown in Fig. 1. Prior to adsorption, both PVA/PAA and NiFeAl-LDHs/PVA/PAA consisted of randomly oriented smooth fibers without beads. The average diameters of PVA/PAA fibers and NiFeAl-LDHs/PVA/PAA were 333.53 and 235.27 nm, respectively. The evident particles of LDHs were observed on the nanofiber surface of NiFeAl-LDHs/PVA/PAA. The deposit on the nanofiber surface increased the adsorption sites.

Hydrophilicity performance of an adsorbent material is significant in view of mass diffusion on the interface of solid–liquid phase. The hydrophilicity of PVA/PAA and NiFeAl-LDHs/PVA/PAA was verified using water contact angle. Figure 2a showed the contact angle change with time. The contact angle for PVA/PAA decreased from 23.5° to 12° from 0.4 to 2 s. During the same time, the contact angle for NiFeAl-LDHs/PVA/PAA decreased from 37° to 21.5°. The change in hydrophilicity performance illustrated the successful introduction of NiFeAl-LDHs composite.

The FT-IR spectrum of NiFeAl-LDHs, PVA/PAA and NiFeAl-LDHs/PVA/PAA are shown in Fig. 2b. One can see that the FT-IR spectrum of NiFeAl-LDHs/PVA/PAA was a superposition of that of NiFeAl-LDHs and PVA/PAA. In

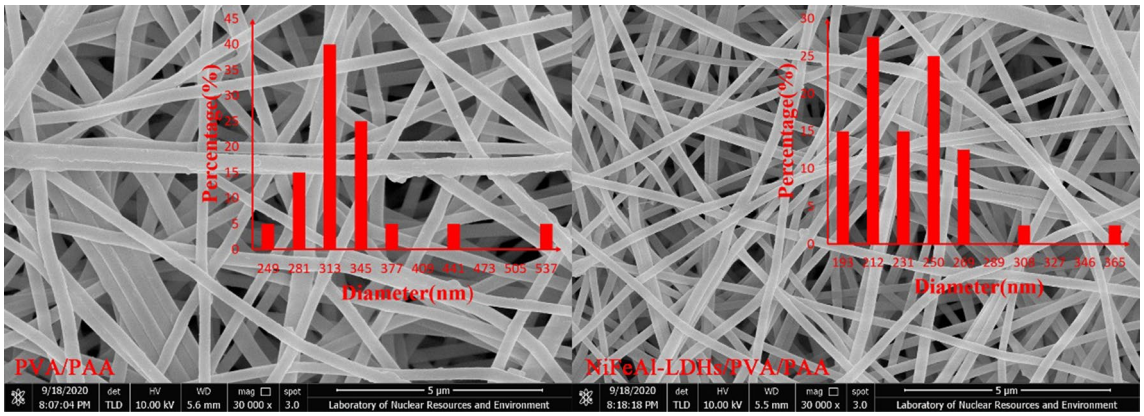

Fig. 1 SEM images of PVA/PAA (**a**) and NiFeAl-LDHs/PVA/PAA (**b**)

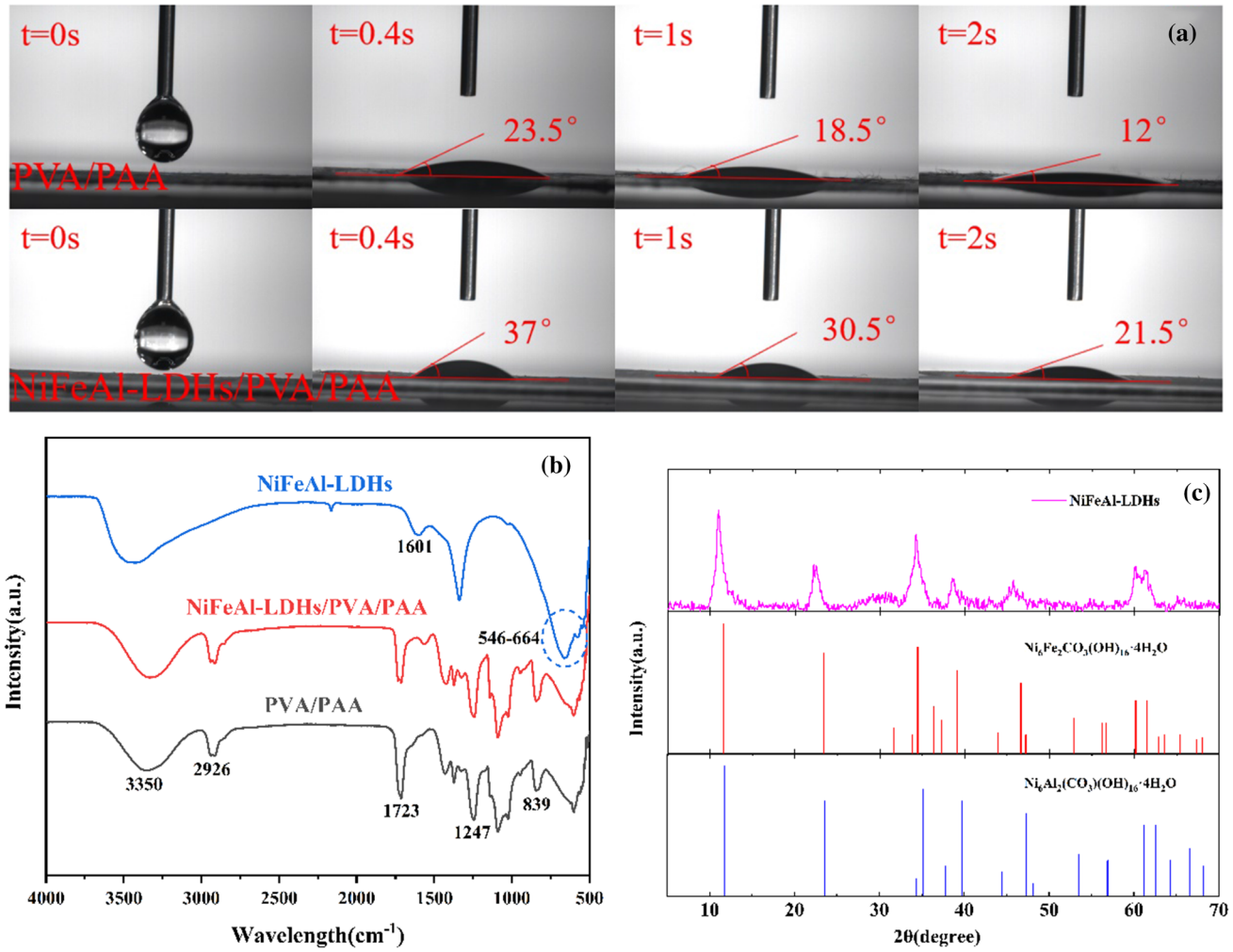

Fig. 2 **a** the water contact angle of PVA/PAA and NiFeAl-LDHs/PVA/PAA; **b** FT-IR spectra; **c** XRD patterns of NiFeAl-LDHs

detail, 3350, 2926, 839, 1247 and 1723 cm^{-1} were assigned as stretching vibration of hydroxy group, C-H bond in the alkyl, C-H bending vibration, C–O–C stretching vibration and C = O stretching vibration peak of the ester group produced by thermal crosslinking, respectively. PVA/PAA and NiFeAl-LDHs/PVA/PAA have different chemical functional

groups at 1601 cm^{-1}. The peak should be the interlayer H_2O in the doped NiFeAl-LDHs, indicating that NiFeAl-LDHs have been doped into PVA/PAA [45]. The peaks at 546 to 664 cm^{-1} in the low wavenumbers of the spectrum were attributed to the bending and tensile vibration of M–O/M-OH (M = Ni, Fe and Al) bonds [46].

The material composition and crystal form of the synthesized LDHs were determined by XRD. Figure 2c showed the XRD spectrum of NiFeAl-LDHs. As shown in the figure, the spectrum line's trend was consistent with that reported in the previous literature, indicating that the synthesized substance was NiFeAl-LDHs with a layered structure [43]. As it was shown, the characteristic peak was consistent with reevesite $Ni_6Fe_2(CO_3)(OH)_{16}{\cdot}4H_2O$ (PDF NO.26–1286) and takovite $Ni_6Al_2(CO_3)(OH)_{16}{\cdot}4H_2O$ (PDF NO.15–0087) [47].

The chemical composition and state of the NiFeAl-LDHs/PVA/PAA before and after the adsorption were studied by XPS (Fig. 3). Obviously, NiFeAl-LDHs/PVA/PAA have the main elements C, O, Ni, Fe, and Al, but also the emergence of a new peak U after the adsorption. As shown in Fig. 3b, the peaks at 381.3 and 392.1 eV belonged to U $4f_{7/2}$ and U $4f_{5/2}$ respectively, and the binding energy difference between the two peaks is 10.8 eV, which was consistent with the characteristics of uranium peak. In addition, Fig. 3c, d and e showed the C 1 s, O 1 s and Ni 2p spectra, respectively. It can be seen from the figure that the peak at 531.51 eV in the O1s spectrum of NiFeAl-LDHs/PVA/PAA before adsorption was considered to be Fe–O, Ni^{2+}–O in the metal hydroxide and C = O bond of the carboxyl group on PAA. And the peak at 533.20 eV belonged to the O–H bond on the hydroxide. After uranium is adsorbed, the binding energy of the two peaks were reduced, indicating that a stable O-U chemical bond has been formed between the hydroxide and the uranyl ion, and the uranium has been successfully separated from the solution. The binding energy of the three peaks in C 1 s after adsorption were increased compared with that before adsorption. It is possible that the O–H bond on the organic fiber substrate was also bound to uranyl ion to form O–U bond, the charge density on the O–H bond was transferred to the organic carbon chain, which resulted in the increase of the bond energy on the carbon chain, indicating that PAA and PVA are also involved in the adsorption of uranium. Ni $2p_{3/2}$ had three peaks after deconvolution in the Ni 2p spectrum. The two peaks at 855.6 and 857.1 eV were considered to be Ni^{2+}-O and Ni^{3+}-O bonds respectively, while the peak at 861.9 eV was the shake-up satellite peak. After adsorption of uranium, the binding energies of the three peaks at Ni $2p_{3/2}$ were only slightly reduced, which indicated that adsorption of uranium has no effect on the charge density of Ni. The chemical composition of LDHs can be represented by the general formula $[M^{II}_{1-x}M^{III}_{x}(OH)_2]^{x+}[A^{n-}]_{x/n}{\cdot}mH_2O$, where M^{II} and M^{III} represent divalent (Ni^{2+}, Mg^{2+}, Co^{2+} and Zn^{2+})and trivalent (Fe^{3+} and Al^{3+}) metal cations, A^{n-} represents interlayer anions (NO_3^-, CO_3^{2-} and Cl^-), x is the molar ratio of $M^{II}/(M^{II}+M^{III})$, and m is the molar of water [48]. U(VI) not only be combined with hydroxyl and carboxyl groups on the nanofibers, but also with hydroxyl in the interlayer of LDHs during the adsorption process. The possible adsorption mechanism was shown in Fig. 4.

The stress–strain curve shown in Fig. 5 displayed that 30% strain for PVA/PAA yielded 13.67 MPa stress, while 115% strain of NiFeAl-LDHs/PVA/PAA corresponded 16.22 MPa stress. And the corresponding Young's Modulus were 182.49 and 47.77 MPa respectively, the Young's Modulus of PVA/PAA decreased by more than 380% after adding NiFeAl-LDHs. It was an unexpected result that the additional inorganic particle substance of LDHs actually intensified, not weakened the mechanical strength of the final product.

pH at different ionic strength

Since the pH of most uranium-containing wastewater and seawater located in the pH range of 4.5–8.0, effect of the pH on the adsorption was studied. The result is shown in Fig. 6a. It is obvious that q_e of NiFeAl-LDHs/PVA/PAA, NiFeAl-LDHs and PVA/PAA increased as pH increased from 4.5 to 6.0 and subsequently decreased as pH increased from 6.0 to 8.0. The turning point occurred at pH 6.0 yielded the maximum adsorption capacity 35.68 mg/g for PVA/PAA, 77.25 mg/g for NiFeAl-LDHs and 122 mg/g for NiFeAl-LDHs/PVA/PAA. The distribution of U(VI) species and the surface charge of adsorbent in solution are affected by the change of pH. Figure 6b showed the distribution of U(VI) species at pH 1–10. U(VI) species dominating existence forms of positive charge ($((UO_2)_3(OH)_5^+$ and $(UO_2)_4(OH)_7^+$) at pH 6.0, while $(UO_2)_3(OH)_7^-$ and $UO_2(OH)_3^-$ were dominating existence forms under alkaline condition. Figure 6c showed the zeta potentials of PVA/PAA, NiFeAl-LDHs and NiFeAl-LDHs/PVA/PAA in different pH. It can be seen that the surface of PVA/PAA, NiFeAl-LDHs and NiFeAl-LDHs/PVA/PAA were all negative charges at pH 6.0. Therefore, the maximum adsorption capacity at pH 6.0 ascribes to the electrostatic attraction to U(VI).

The significantly synergistic effect was found that q_e of NiFeAl-LDHs/PVA/PAA was evidently higher than single NiFeAl-LDHs and PVA/PAA. The effect was resulted from (1) the hydrophilicity structure of PVA/PAA provided numerous diffusion channel for uranium species; (2) the nanofiber structure ensured sufficient contact between uranium species and adsorption site; (3) NiFeAl-LDHs particles totally spread out nanofibers rather than conglomeration; (4) NiFeAl-LDHs/PVA/PAA has more electrostatic attraction to U(VI) ascribes to more negative surface charges at pH 6.0.

In addition, q_e of NiFeAl-LDHs/PVA/PAA varied slightly with the change in $NaClO_4$ concentration of 0.1–0.5 mol/L at

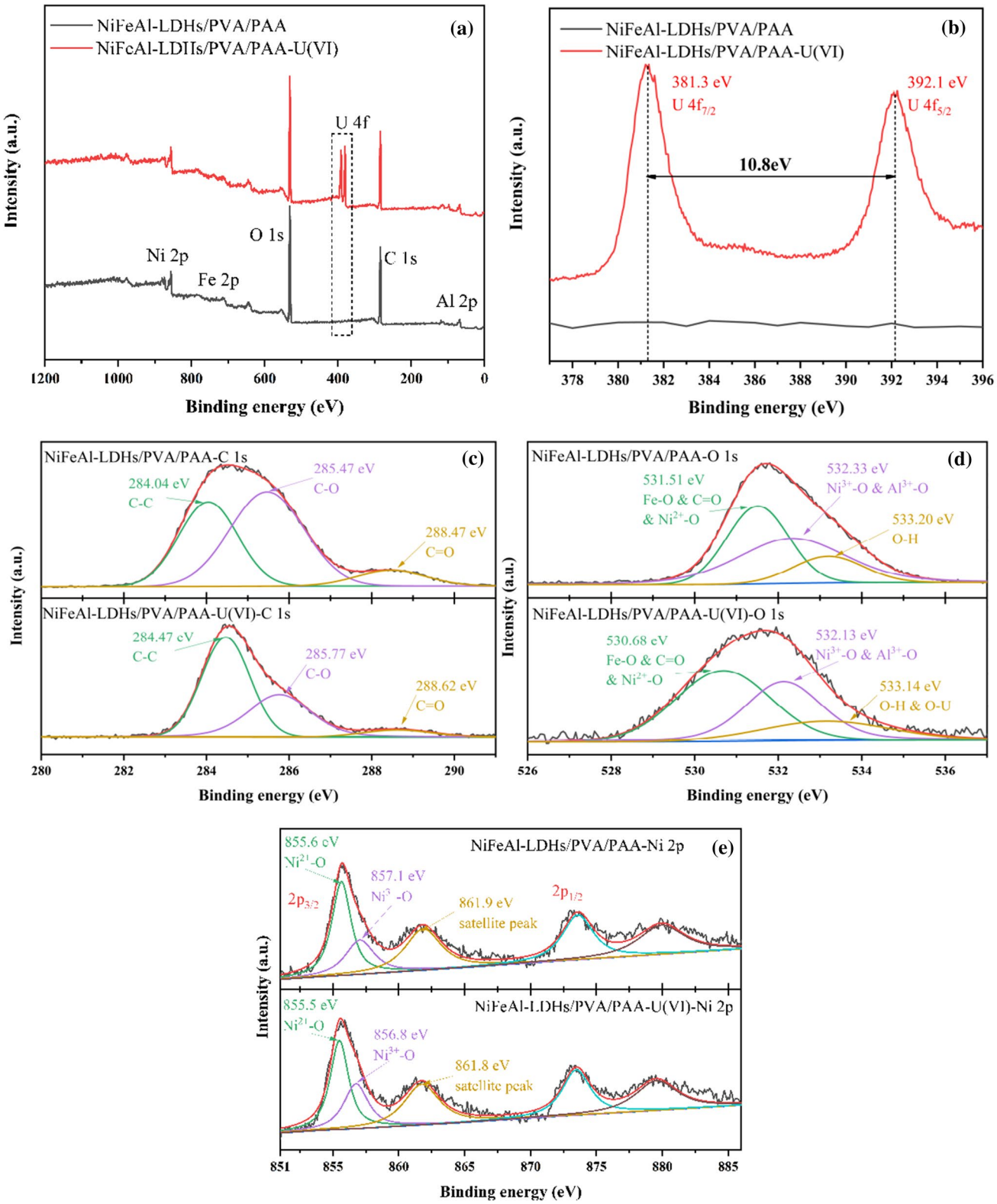

Fig. 3 The XPS spectra **a**, U 4f **b**, C 1 s **c**, O 1 s **d** and Ni 2p **e** of NiFeAl-LDHs/PVA/PAA before and after uranium adsorption

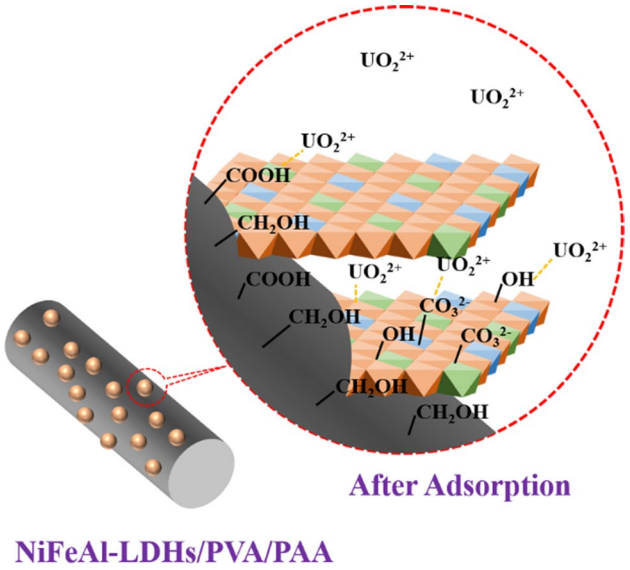

Fig. 4 Adsorption mechanism of uranyl ion on NiFeAl-LDHs/PVA/PAA

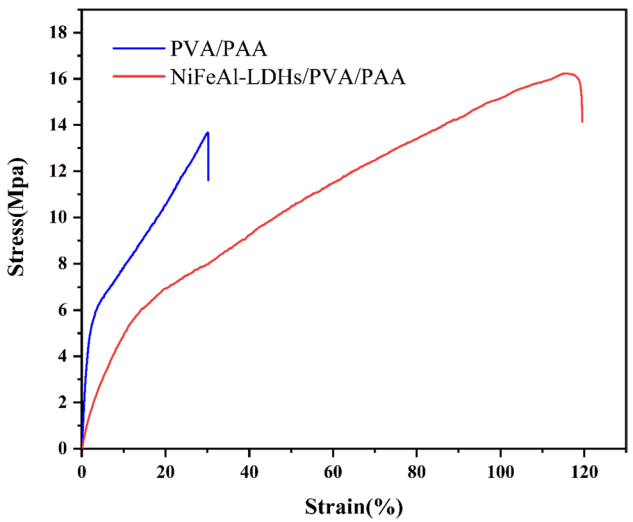

Fig. 5 The stress–strain curve of PVA/PAA and NiFeAl-LDHs/PVA/PAA

6.0. The consequence indicated ionic strength showed little influence on NiFeAl-LDHs/PVA/PAA. It was displayed that uranium adsorbed on NiFeAl-LDHs/PVA/PAA at pH 6.0 adopted the way of inner-sphere surface complex.

Isotherms

As shown in the Fig. 7a, with the initial uranium concentration increasing from 10 to 200 mg/L, the adsorption capacity of both fibers for uranium from enhanced to then gradually reaches the equilibrium state. The maximum adsorption capacity of PVA/PAA and NiFeAl-LDHs/PVA/PAA were 48.51 and 174.30 mg/g, respectively. The mass transfer resistance decreased with the increase of the initial concentration of uranium, and many adsorption sites on the fiber gradually combine with uranium until the adsorption capacity of the fiber remains unchanged after saturation.

To study the adsorption mechanism of uranium on NiFeAl-LDHs/PVA/PAA, Langmuir, Freundlich and Duninin–Radushkevich isotherm models were used to present the relationship between equilibrium concentration and equilibrium adsorption capacity. The Langmuir model assumes that the molecules are monolayer adsorbed on the solid surface, and estimates the maximum monolayer adsorption capacity of the adsorbent. The nonlinear Langmuir model can be expressed by Eq. (2):

$$q_e = \frac{K_L q_m C_e}{1 + K_L C_e} \tag{2}$$

where q_m (mg/g) is the maximum monolayer adsorption capacity, K_L (L/mg) is the Langmuir isotherm model constant, and C_e (mg/L) is the equilibrium uranium concentration.

The dimensionless factor R_L value in the Langmuir isotherm model can determine the advantage of the adsorption process, which can be divided into four situations: irreversible adsorption ($R_L = 0$), favorable adsorption ($0 < R_L < 1$), linear adsorption ($R_L = 1$) and unfavorable adsorption ($R_L > 1$). The R_L value can be calculated by Eq. 3:

$$R_L = \frac{1}{1 + K_L C_0} \tag{3}$$

The Freundlich isotherm model considers that the solid surface is multilayer adsorption and heterogeneous, and there are different adsorption sites on the surface. The non-linear Freundlich model was shown in Eq. (4):

$$q_e = K_F C_e^{1/n} \tag{4}$$

where K_F [$(mg \cdot g^{-1})$ $(L \cdot mg^{-1})^{1/n}$] Freundlich isotherm model constant and n is a characteristic constant associated with the intensity of adsorption.

The Duninin–Radushkevich isotherm model can be used to estimate the average free energy (E (kJ/mol)) of adsorption on heterogeneous surfaces. When the value of E was between 1–8 kJ/mol, the adsorption mechanism was physical adsorption, and in the range of 8–16 kJ/mol, the adsorption mechanism was chemical adsorption. The non-linear D-R mathematical expressions, related parameters and the average free energy formulas are shown in Eqs. (5), (6) and. (7), respectively:

$$q_e = q_m e^{-K_{DR}\varepsilon^2} \tag{5}$$

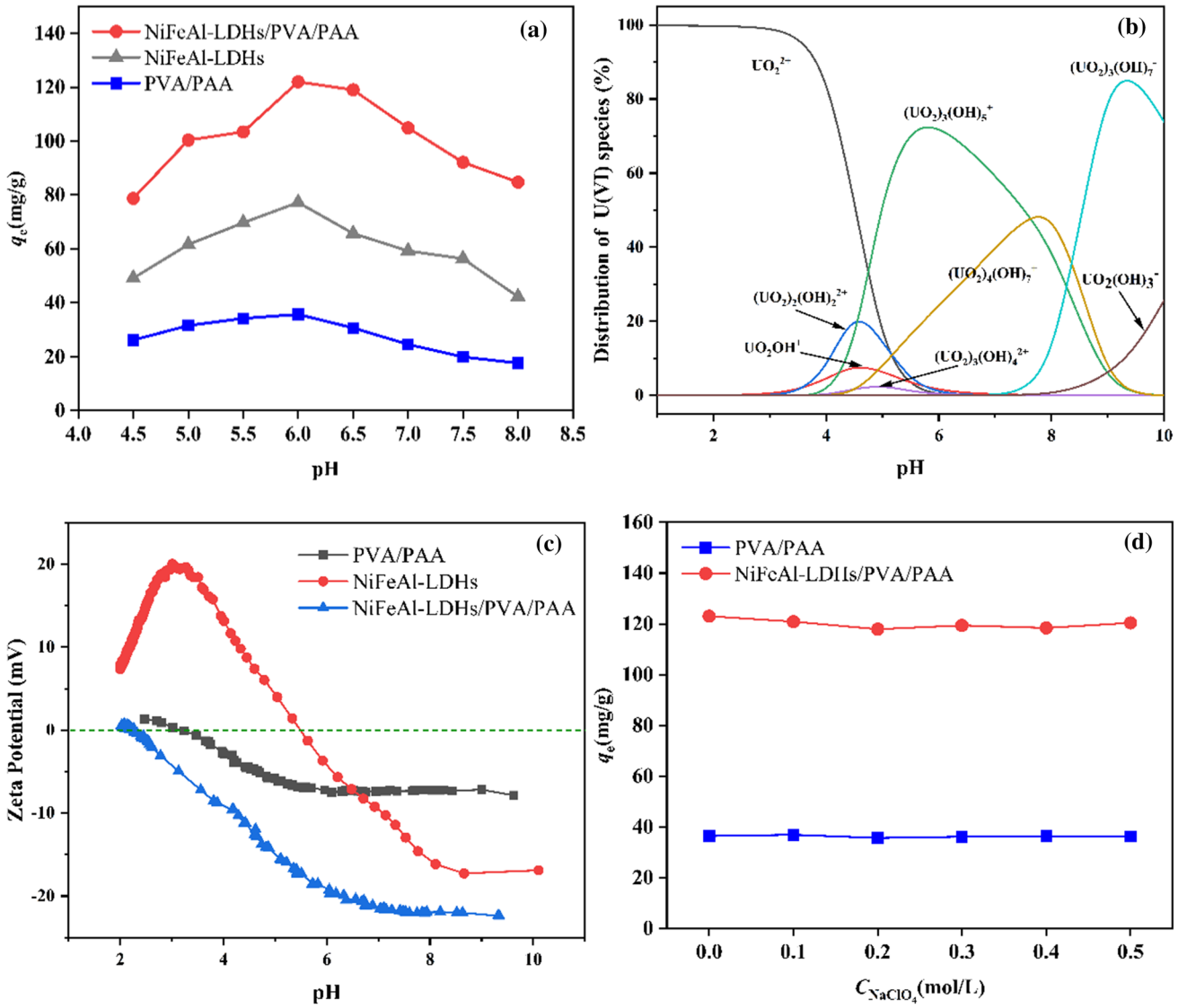

Fig. 6 **a** Effect of pH on uranium adsorption capacity of PVA/PAA, NiFeAl-LDHs and NiFeAl-LDHs/PVA/PAA; **b** The distribution of aqueous U(VI) species in the U(VI)-NO_3^- system; **c** The zeta potential of PVA/PAA, NiFeAl-LDHs and NiFeAl-LDHs/PVA/PAA; **d** Effect of ion strength on uranium adsorption capacity of PVA/PAA and NiFeAl-LDHs/PVA/PAA

$$\varepsilon = RT\ln(1+\frac{1}{C_e}) \tag{6}$$

$$E = \frac{1}{\sqrt{-2K_{DR}}} \tag{7}$$

where q_e (mg/g) and q_m (mg/g) are the adsorption capacity at equilibrium and the maximum adsorption capacity, respectively, and K_{DR} ((mol/kJ)^2) and ε (kJ/mol) are the Duninin–Radushkevich isotherm model constants.

Figure 7a and b showed the Langmuir, Freundlich and Duninin-Radushkevich isotherm model curves, respectively. The calculation results of the relevant parameters of all isotherm models were shown in Table 1. From the table data, the adsorption process of PVA/PAA and NiFeAl-LDHs/PVA/PAA for uranium were most consistent with the Langmuir model, and the correlation coefficients R^2 are 0.995 and 0.997 respectively, which are higher than Freundlich model and Duninin-Radushkevich model. The theoretical maximum adsorption capacities of PVA/PAA and NiFeAl-LDHs/PVA/PAA calculated by the Langmuir model are 55.64 mg/g and 203.32 mg/g, respectively. The above results indicated that the adsorption mechanism of PVA/PAA and NiFeAl-LDHs/PVA/PAA accords with the Langmuir model. Therefore, the adsorption of uranium above both fibers were belong to chemical monolayer adsorption. The R_L values calculated in Table 2 were between 0 and 1, which indicated

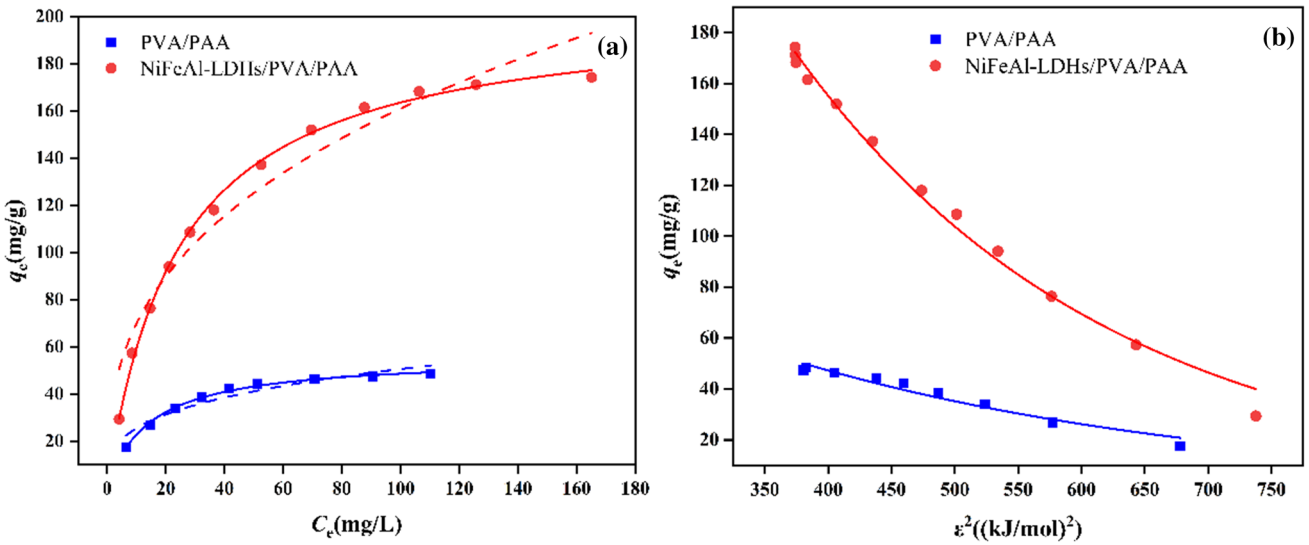

Fig. 7 **a** Non-linear Langmuir (full line) and Freundlich (dotted line) adsorption isotherm models; **b** Non-linear Duninin–Radushkevich isotherm model

Table 1 Adsorption isotherms parameters of U(VI) adsorption onto PVA/PAA and NiFeAl-LDHs/PVA/PAA

Adsorbent	Langmuir isotherm			
	K_L (L/mg)	q_m (mg/g)		R^2
PVA/PAA	0.069	55.64		0.995
NiFeAl-LDHs/PVA/PAA	0.041	203.32		0.997
Adsorbent	Freundlich isotherm			
	n	K_F (mg·g^{-1}) (L·mg^{-1})$^{1/n}$		R^2
PVA/PAA	3.3537	12.808		0.910
NiFeAl-LDHs/PVA/PAA	2.756	30.270		0.945
Adsorbent	Duninin–Radushkevich isotherm			
	q_m (mg/g)	K_{DR} ((mol/kJ)^2) × 10^3	E (kJ/mol)	R^2
PVA/PAA	36.62	2.95	13.019	0.952
NiFeAl-LDHs/PVA/PAA	184.30	4.02	11.152	0.991

that PVA/PAA and NiFeAl-LDHs/PVA/PAA were favorable for adsorption of uranium from wastewater. In addition, the average free energy E values calculated by the Duninin-Radushkevich model were in the range of 816 kJ/mol, which can also prove that the adsorption mechanism of both fibers on uranium were chemical adsorption. The adsorption performance of NiFeAl-LDHs/PVA/PAA to uranium was compared with other adsorbents as shown in Table 3.

Kinetics

The influence of contact time on uranium adsorption capacity of PVA/PAA and NiFeAl-LDHs/PVA/PAA were shown in Fig. 8a. With contact time gradually increasing from 10 to 210 min, the adsorption capacity of PVA/PAA and NiFeAl-LDHs/PVA/PAA gradually increased until equilibrium, and the maximum adsorption capacity was 44.01 mg/g and 84.13 mg/g, respectively. The adsorption sites on the fiber surface combine with uranyl ion at the beginning of adsorption and quicken the adsorption speed. When the adsorption sites on the surface of the fiber were gradually occupied, uranyl ions permeated into the inner layer of the fiber, the adsorption was gradually blocked. Finally, the adsorption capacity of the fiber reached saturation.

To further understand the adsorption mechanism, the adsorption processes of uranyl ions on PVA/PAA and NiFeAl-LDHs/PVA/PAA were studied by pseudo-first-order

Table 2 Langmuir isotherm model parameters, R_L (T = 298 K)

Uranium concentration (mg/L)	R_L	
	NiFeAl-LDHs/PVA/PAA	PVA/PAA
10	0.709	0.592
20	0.549	0.420
30	0.448	0.326
40	0.379	0.266
50	0.328	0.225
60	0.289	0.195
80	0.234	0.153
100	0.196	0.127
120	0.169	0.108
140	0.148	–
160	0.132	–
200	0.109	–

model, pseudo-second-order model and intra-particle diffusion model.

The mathematical expression of the non-linear pseudo-first-order model was shown in Eq. (8):

$$q_t = q_e\left(1 - e^{-k_1 t}\right) \tag{8}$$

The mathematical expression of the non-linear pseudo-second-order model was shown in Eq. (9):

$$q_t = \frac{q_e^2 k_2 t}{1 + q_e k_2 t} \tag{9}$$

The mathematical expression of the intra-particle diffusion model was shown in Eq. (10):

$$q_t = k_i t^{1/2} + C \tag{10}$$

where q_t (mg/g) and q_e (mg/g) are the adsorption capacities of uranium on PVA/PAA and NiFeAl-LDHs/PVA/PAA

Table 3 Comparison of uranium adsorption capacity between NiFeAl-LDHs/PVA/PAA and other adsorbents

Adsorbents	pH	T/K	q_m (mg/g)	References
Graphene oxide nanoribbons aerogel	4.5	298	430.6	[49]
Active carbon/polyacrylonitrile	4.0	303	16.41	[50]
Phosphate group-functionalized biochars	4.0	298	229.2	[51]
Mg-Fe layered double hydroxides	5.0	298	710.0	[52]
2-phosphonobutane-1,2,4-tricarboxylic acid-decorated chitosan-coated magnetic silica nanoparticles	4.0	298	83.16	[53]
Phytic acid functionalized microwave-assisted hydrothermal carbon	6.0	298	382.2	[54]
Three-dimensional fiber-network chitosan films	5.0	298	196.74	[55]
Flower-like greigite Fe_3S_4 microcrystal	5.0	298	423.0	[56]
Magnetized HNO_3-treated activated carbon	5.0	298	688.03	[57]
NiFeAl-LDHs/PVA/PAA	6.0	298	203.32	This work

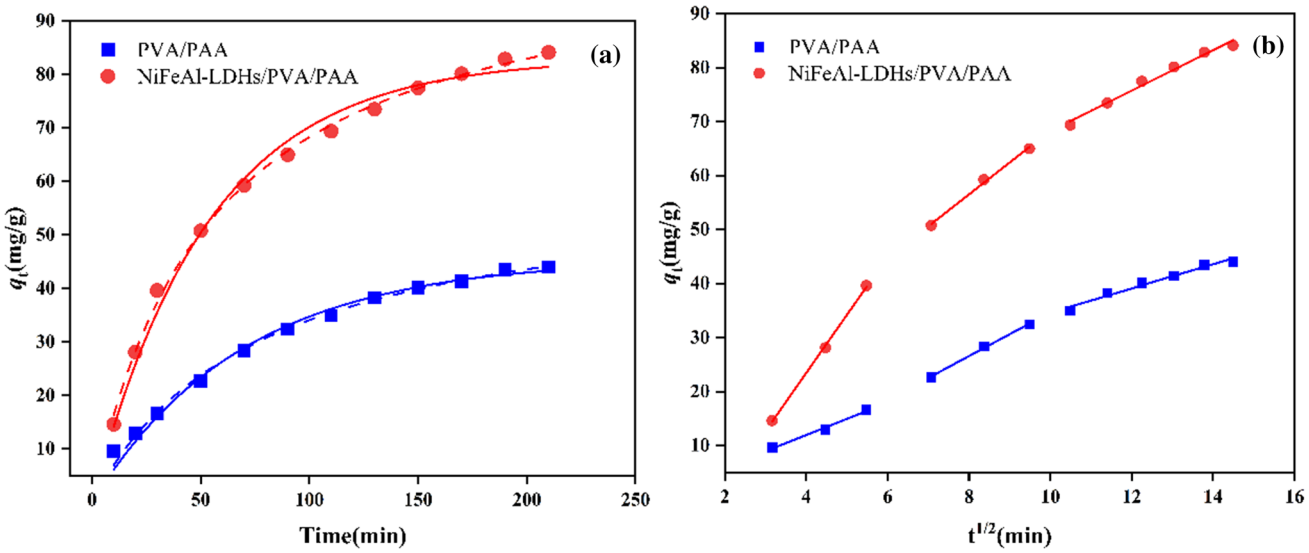

Fig. 8 **a** Non-linear the pseudo-first-order (full line) and pseudo-second-order (dotted line) kinetics model; **b** intra-particle diffusion model

at time t and equilibrium, respectively, and k_1 (min^{-1}), k_2 (g/(mg·min)) and k_i (mg/g·$min^{1/2}$) are the adsorption rate parameters of the pseudo-first-order, pseudo-second-order and intra-particle diffusion kinetics model, respectively.

The pseudo-first-order model and the pseudo-second-order model were shown in Fig. 8a, and the calculation results were listed in Table 4. As the chart shows, the experimental data accorded closely with the pseudo-second-order model, the correlation coefficients R^2 of PVA/PAA and NiFeAl-LDHs/PVA/PAA lived up to 0.994 and 0.998 respectively, which were higher than the correlation coefficient R^2 of the pseudo-first-order model. The uranium adsorption capacity of PVA/PAA and NiFeAl-LDHs/PVA/PAA calculated by the pseudo-second-order simulation is 60.26 and 105.63 mg/g, which are close to the experimentally detected uranium adsorption capacity of 44.01 and 84.13 mg/g. Therefore, the adsorption mechanism of uranyl ion on NiFeAl-LDHs/PVA/PAA was more in line with the pseudo-second-order kinetic model, which belonged to chemisorption.

The intra-particle diffusion model was shown in Fig. 8b. It can be seen from the figure that the process of uranium adsorption by fiber can be divided into three stages: fiber surface adsorption stage, adsorbate intra-particle diffusion stage and adsorption equilibrium stage [48]. In the first stage, the adsorption rate was the fastest, and uranyl ions were quickly adsorbed by the adsorption sites on the fiber surface; in the second stage, the adsorption rate slowed down, and the adsorption sites on the fiber surface decreased, and the uranyl ions penetrated the fiber and were gradually absorbed; in the third stage, the adsorption rate was almost zero, the adsorption was close to equilibrium, and the adsorption capacity remained almost unchanged. Besides, the straight line fitted in the second stage did not match the origin of coordinates, indicating that the adsorption process was not only controlled by the intra-particle diffusion, but also affected by other adsorption mechanisms.

Thermodynamics

Figure 9a showed the effect of temperature on the uranium adsorption capacity of PVA/PAA and NiFeAl-LDHs/PVA/PAA. As can be seen from the diagram, the adsorption capacity of uranium by both fibers increased with the increase of temperature, indicating that the adsorption process of uranium by the PVA/PAA and NiFeAl-LDHs/PVA/PAA were endothermic. The effect of temperature on the adsorption process can be studied by calculating the standard enthalpy ($\Delta H°$), standard entropy ($\Delta S°$) and standard free energy ($\Delta G°$). These thermodynamic parameters can be calculated by Eq. (11) and Eq. (12):

$$\ln K_d = \frac{\Delta S°}{R} - \frac{\Delta H°}{RT} \tag{11}$$

$$\Delta G° = \Delta H° - T\Delta S° \tag{12}$$

where K_d is the thermodynamic adsorption equilibrium constant, R (8.314 J/(mol·K)) is the gas constant, and T (K) is the thermodynamic temperature.

Figure 9b showed a linear plot of the fitted thermodynamic parameters ln K_d and 1/T, and the calculation results of the relevant parameters were listed in Table 5. From the data in Table 3, the adsorption thermodynamics of the PVA/PAA and NiFeAl-LDHs/PVA/PAA had higher fitting degrees, and the correlation coefficient R^2 were 0.963 and 0.985, respectively. The negative value of standard enthalpy change was considered proof of that the fiber adsorption was endothermic reaction; The positive values of standard entropy change was deemed that the degree of

Table 4 The parameters of the pseudo-first-order, pseudo-second-order kinetics and intra-particle diffusion model

Adsorbent	Pseudo-first-order kinetics		
	q_e (mg/g)	k_1 (min^{-1})	R^2
PVA/PAA	45.47	0.014	0.987
NiFeAl-LDHs/PVA/PAA	83.06	0.019	0.989
Adsorbent	Pseudo-second-order kinetics		
	q_e (mg/g)	k_2 (g/(mg·min))	R^2
PVA/PAA	60.26	2.164×10^{-4}	0.994
NiFeAl-LDHs/PVA/PAA	105.63	1.730×10^{-4}	0.998
Adsorbent	Intra-particle diffusion		
	k_2 (mg/g·$min^{1/2}$)	C	R^2
PVA/PAA	4.053	−5.840	0.994
NiFeAl-LDHs/PVA/PAA	5.916	9.183	0.990

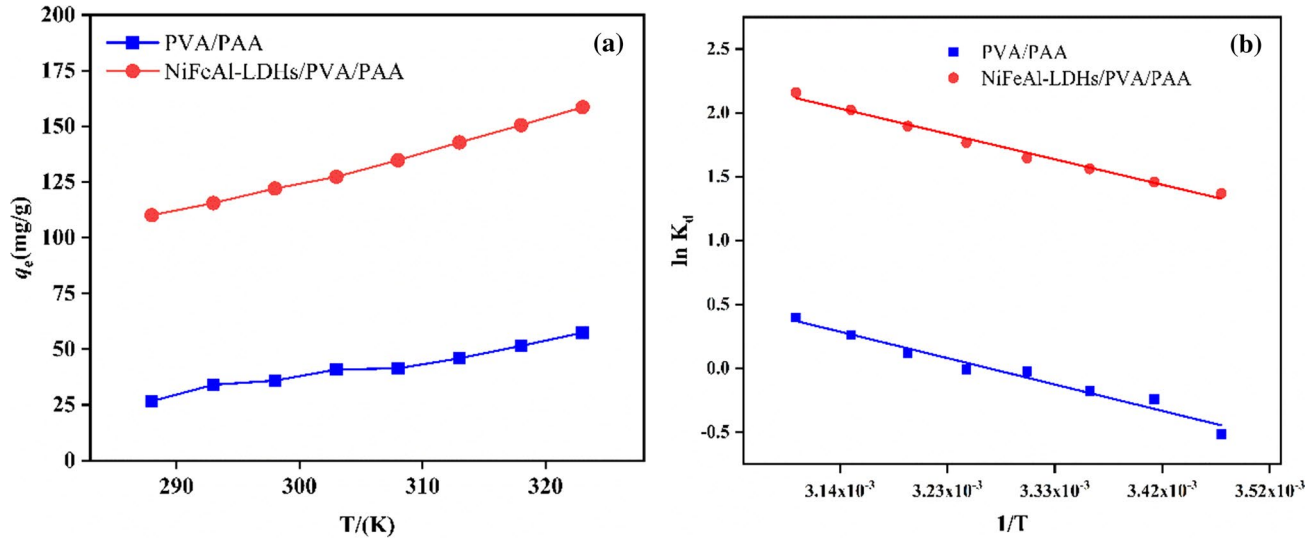

Fig. 9 **a** Effect of temperature on uranium adsorption capacity of PVA/PAA and NiFeAl-LDHs/PVA/PAA; **b** the function relationship between ln K_d and 1/T

Table 5 Thermodynamic parameters of U(VI) adsorption on PVA/PAA and NiFeAl-LDHs/PVA/PAA

Adsorbent	Temperature (K)	$\Delta G°$ (kJ/mol)	$\Delta H°$ (kJ/mol)	$\Delta S°$ (J/mol)	R^2
PVA/PAA	288	−38.0173	−17.4195	71.5202	0.963
	293	−38.3749			
	298	−38.7325			
	303	−39.0901			
	308	−39.4477			
	313	−39.8053	–		
	318	−40.1629			
	323	−40.5205			
NiFeAl-LDHs/PVA/PAA	288	−35.0934	−18.0809	59.0711	0.985
	293	−35.3887			
	298	−35.6841			
	303	−35.9795			
	308	−36.2748			
	313	−36.5702			
	318	−36.8655			
	323	−37.1609			

disorder in the adsorption process increases and the reaction was easy to proceed. The positive values of standard free energy were regarded as the adsorption process was spontaneous and feasible. The absolute value of standard free energy increased with the increase of temperature, indicating that the higher the temperature, the better the adsorption effect.

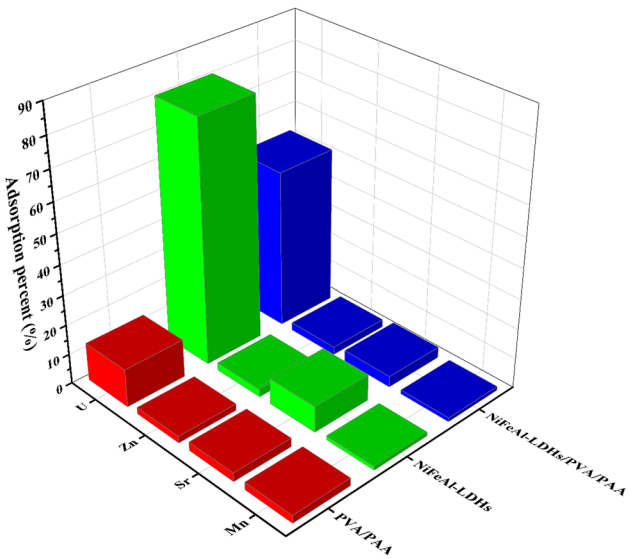

Fig. 10 The ion selectivity of PVA/PAA, NiFeAl-LDHs and NiFeAl-LDHs/PVA/PAA to the co-existing ions U, Zn, Sr, Mn

Co-existing cations

The ion selectivity of PVA/PAA, NiFeAl-LDHs and NiFeAl-LDHs/PVA/PAA to 4 co-existing ions of U, Zn, Sr and Mn was measured. It can be seen from Fig. 10 that the adsorption percent of U by PVA/PAA was the similarity with other ions, while the adsorption percent of U (greater than 50%) by NiFeAl-LDHs and NiFeAl-LDHs/PVA/PAA were significantly higher than other ions (less than 10%). NiFeAl-LDHs has good selectivity to uranium, which may be due to the matching of the interlayer spacing of NiFeAl-LDHs

with the diameter of uranyl ions, which can keep uranyl ions between the layers. Although the adsorption percent of uranium on NiFeAl-LDHs/PVA/PAA (52.4%) is lower than that of NiFeAl-LDHs (80.8%), but much higher than that of PVA/PAA (12.8%), indicating that the doped of NiFeAl-LDHs in PVA/PAA can significantly enhance the adsorption selectivity of composite nanofibers for uranium.

Regeneration and reusability

Different eluents were used to evaluate the uranium elution performance of PVA/PAA and NiFeAl-LDHs/PVA/PAA. As shown in Fig. 11a, 1 mol/L HCl, H_2SO_4, HNO_3, $NaCO_3$ and EDTA were used to elute uranium adsorbed on the PVA/PAA and NiFeAl-LDHs/PVA/PAA. Among them, 1 mol/L HCl had the best elution effect on the fiber, reaching 98.23 and 99.34% respectively. The abundant free H^+ in the strong acid can not only combine with the oxygen in the carboxyl groups and hydroxyl groups on the fiber, but also inhibit the activity of layered double hydroxides, which will be constrained to the adsorption of uranium and increase the elution rate. However, the anions in the H_2SO_4 and HNO_3 solutions were easily complexed with uranyl ions, which will reduce the elution rate, hence best results for the elution effect with HCl.

Figure 11b showed the effect of five adsorption–desorption cycles on the adsorption capacity and desorption efficiency of NiFeAl-LDHs/PVA/PAA. It can be seen from the figure that after five adsorption desorption cycles, the adsorption capacity of NiFeAl-LDHs/PVA/PAA decreased from 119.45 to 71.15 mg/g, which decreased by nearly 40%. The strong acid solution will destroy the structure of the layered double hydroxide after multiple elutions, thereby affecting the adsorption and desorption performance of the nanofibers. However, the desorption rate dropped from 99.36% to 86.76% and still maintained high desorption efficiency, shedding light on that NiFeAl-LDHs/PVA/PAA could be an efficient sorbent to uptake U(VI) repeatedly.

Conclusion

In summary, NiFeAl-LDHs, PVA and PAA were used as raw materials to prepare super-hydrophilic and flexible NiFeAl-LDHs/PVA/PAA composite nanofiber through electrospinning and thermal crosslinking. The added NiFeAl-LDHs significantly improved the uranium adsorption performance and mechanical properties of PVA/PAA. The structure and textural properties of NiFeAl-LDHs/PVA/PAA were characterized by SEM, FT-IR, XPS and universal tensile testing machine, and various factors on the adsorption behaviour of the adsorbent was studied from static and dynamic adsorption. The results show that the kinetics of the adsorption process conforms to the pseudo-second-order model ($R^2 > 0.998$), and the adsorption isotherm data was in accord with the Langmuir model. The adsorption mechanism of the amorphous and uniform NiFeAl-LDHs/PVA/PAA nanofiber for U(VI) is chemisorption. XPS spectroscopy showed that U(VI) not only be combined with hydroxyl and carboxyl groups on the nanofibers, but also with hydroxyl in the interlayer of LDHs during the adsorption process. The theoretical maximum adsorption capacity for U(VI) was 203.32 mg/g at pH 6.0. Thermodynamics showed that the adsorption of uranium by NiFeAl-LDHs/PVA/PAA was endothermic and

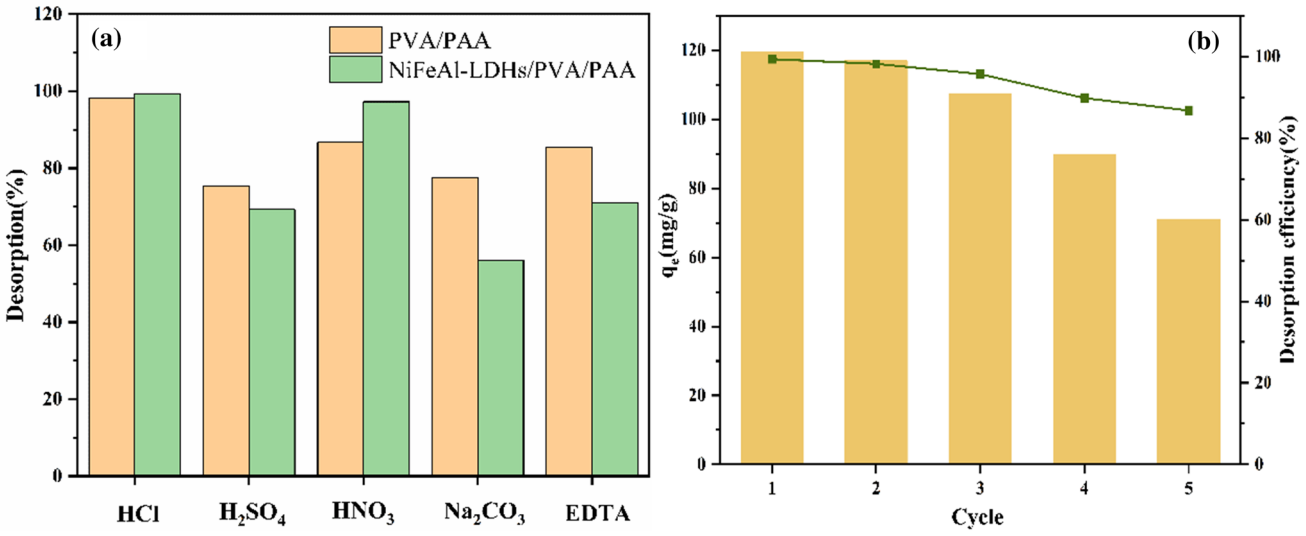

Fig. 11 **a** Elution of U(VI) on the nanofibers by 1 mol/L HCl, H_2SO_4, HNO_3, $NaCO_3$ and EDTA; **b** the effect of five adsorption–desorption cycles on the adsorption capacity and desorption efficiency of NiFeAl-LDHs/PVA/PAA

spontaneous. After five adsorption–desorption cycles, the NiFeAl-LDHs/PVA/PAA can still maintain a high adsorption capacity for U(VI). Therefore, NiFeAl-LDHs/PVA/PAA can be an ideal choice for uranium adsorption in practical applications.

Acknowledgements The present work was financially supported by National Natural Science Foundation of China (21866003, 22066001).

References

1. Wang S, Ran Y, Lu B, Li J, Kuang H, Gong L, Hao Y (2020) A Review of uranium-induced reproductive toxicity. Biol Trace Elem Res 196(1):204–213
2. Gao N, Huang Z, Liu H, Hou J, Liu X (2019) Advances on the toxicity of uranium to different organisms. Chemosphere 237:124548
3. Bjørklund G, Pivina L, Dadar M, Semenova Y, Rahman MM, Chirumbolo S, Aaseth J (2020) Depleted uranium and Gulf War Illness: updates and comments on possible mechanisms behind the syndrome. Environ Res 181:108927
4. Faa A, Gerosa C, Fanni D, Floris G, Eyken PV, Lachowicz JI, Nurchi VM (2018) Depleted uranium and human health. Curr Med Chem 25(1):49–64
5. Bjorklund G, Semenova Y, Pivina L, Dadar M, Rahman MM, Aaseth J, Chirumbolo S (2020) Uranium in drinking water: a public health threat. Arch Toxicol 94(5):1551–1560
6. Lourenco J, Marques S, Carvalho FP, Oliveira J, Malta M, Santos M, Goncalves F, Pereira R, Mendo S (2017) Uranium mining wastes: the use of the fish embryo acute toxicity test (FET) test to evaluate toxicity and risk of environmental discharge. Sci Total Environ 605:391–404
7. Ouyang J, Liu Z, Zhang L, Wang Y, Zhou L (2020) Analysis of influencing factors of heavy metals pollution in farmland-rice system around a uranium tailings dam. Process Saf Environ 139:124–132
8. Ouyang J, Liu Z, Ye T, Zhang L (2019) Uranium pollution status and speciation analysis in the farmland-rice system around a uranium tailings mine in southeastern China. J Radioanal Nucl Ch 322(2):1011–1022
9. Selvakumar R, Ramadoss G, Menon MP, Rajendran K, Thavamani P, Naidu R, Megharaj M (2018) Challenges and complexities in remediation of uranium contaminated soils: a review. J Environ Radioactiv 192:592–603
10. Sun Y, Li Y (2021) Application of surface complexation modeling on adsorption of uranium at water-solid interface: A review. Environ Pollut 278:116861
11. Xue G, Yurun F, Li M, Dezhi G, Jie J, Jincheng Y, Haibin S, Hongyu G, Yujun Z (2017) Phosphoryl functionalized mesoporous silica for uranium adsorption. Appl Surf Sci 402:53–60
12. Rosenberg E, Pinson G, Tsosie R, Tutu H, Cukrowska E (2016) Uranium remediation by ion exchange and sorption methods: a critical review various types of solid phase sorbents are studied and evaluated. Johnson Matthey Tech 60(1):59–77
13. Li L, Zhao Y, Jin Y, Linghu W, Chen C, Asiri AM, Marwani HM, Sheng G (2019) Efficient scavenging of uranium (VI) using porous hexagonal boron nitride by a combined process of surface adsorption and induced precipitation crystallization. J Radioanal Nucl Ch 321(3):1035–1044
14. Geran S, Chamelot P, Serp J, Gibilaro M, Massot L (2020) Electrochemistry of uranium in molten LiCl-LiF. Electrochim Acta 355:136784
15. He S, Yang Z, Cui X, Zhang X, Niu X (2020) Fabrication of the novel Ag-doped SnS2@ InVO4 composite with high adsorption-photocatalysis for the removal of uranium (VI). Chemosphere 260:127548
16. Li P, Wang J, Wang Y, Liang J, He B, Pan D, Fan Q, Wang X (2019) Photoconversion of U(VI) by TiO_2: an efficient strategy for seawater uranium extraction. Chem Eng J 365:231–241
17. Wu J, Tian K, Wang J (2018) Adsorption of uranium (VI) by amidoxime modified multiwalled carbon nanotubes. Prog Nucl Energ 106:79–86
18. Lyu P, Wang G, Cao Y, Wang B, Deng N (2021) Phosphorus-modified biochar cross-linked Mg–Al layered double-hydroxide composite for immobilizing uranium in mining contaminated soil. Chemosphere 276:130116
19. Tatarchuk T, Shyichuk A, Mironyuk I, Naushad M (2019) A review on removal of uranium (VI) ions using titanium dioxide based sorbents. J Mol Liquids 293:111563
20. Yang W, Pan Q, Song S, Zhang H (2019) Metal–organic framework-based materials for the recovery of uranium from aqueous solutions. Inorg Chem Front 6(8):1924–1937
21. Wu H, Chi F, Zhang S, Wen J, Xiong J, Hu S (2019) Control of pore chemistry in metal-organic frameworks for selective uranium extraction from seawater. Microporous and Mesoporous Mater 288:109567
22. Gu P, Zhang S, Li X, Wang X, Wen T, Jehan R, Alsaedi A, Hayat T, Wang X (2018) Recent advances in layered double hydroxide-based nanomaterials for the removal of radionuclides from aqueous solution. Environ Pollut 240:493–505
23. Yu S, Wang X, Liu Y, Chen Z, Wu Y, Liu Y, Pang H, Song G, Chen J, Wang X (2019) Efficient removal of uranium(VI) by layered double hydroxides supported nanoscale zero-valent iron: A combined experimental and spectroscopic studies. Chem Eng J 365:51–59
24. Naeem H, Bhatti HN, Sadaf S, Iqbal M (2017) Uranium remediation using modified Vigna radiata waste biomass. Appl Radiat Isotopes 123:94–101
25. Yi Z, Liu J, Zeng R, Liu X, Long J, Huang B (2020) Removal of uranium(VI) from aqueous solution by Camellia oleifera shell-based activated carbon: adsorption equilibrium, kinetics, and thermodynamics. Water Sci Technol 82(11):2592–2602
26. Singhal P, Vats BG, Pulhani V (2020) Magnetic nanoparticles for the recovery of uranium from sea water: challenges involved from research to development. J Ind Eng Chem 90:17–35
27. Calì E, Qi J, Preedy O, Chen S, Boldrin D, Branford WR, Vandeperre L, Ryan MP (2018) Functionalised magnetic nanoparticles for uranium adsorption with ultra-high capacity and selectivity. J Mater Chem A 6(7):3063–3073
28. Zhu F, Zheng YM, Zhang BG, Dai YR (2021) A critical review on the electrospun nanofibrous membranes for the adsorption of heavy metals in water treatment. J Hazard Mater 401:123608
29. Bode-Aluko CA, Pereao O, Ndayambaje G, Petrik L (2016) Adsorption of Toxic Metals on Modified Polyacrylonitrile Nanofibres: A Review. Water Air Soil Poll 228(1):1–11
30. Hu X, Wang Y, Yang JO, Li Y, Wu P, Zhang H, Yuan D, Liu Y, Wu Z, Liu Z (2020) Synthesis of graphene oxide nanoribbons/chitosan composite membranes for the removal of uranium from aqueous solutions. Front Chem Sci Eng 14(6):1029–1038
31. Christou C, Philippou K, Krasia-Christoforou T, Pashalidis I (2019) Uranium adsorption by polyvinylpyrrolidone/chitosan blended nanofibers. Carbohyd Polym 219:298–305
32. Gebru KA, Das C (2017) Removal of Pb (II) and Cu (II) ions from wastewater using composite electrospun cellulose acetate/titanium oxide (TiO_2) adsorbent. J Water Process Eng 16:1–13
33. Wang Y, Zhang Y, Li Q, Li Y, Cao L, Li W (2020) Amidoximated cellulose fiber membrane for uranium extraction from simulated seawater. Carbohyd Polym 245:116627

34. Wang F, Song Y, Liang S, Yu Y, Liang J, Jiang M (2021) Polyamidoxime nanoparticles/polyvinyl alcohol composite chelating nanofibers prepared by centrifugal spinning for uranium extraction. React Funct Polym 159:104812
35. Talebi M, Abbasizadeh S, Keshtkar AR (2017) Evaluation of single and simultaneous thorium and uranium sorption from water systems by an electrospun PVA/SA/PEO/HZSM5 nanofiber. Process Saf Environ 109:340–356
36. Xie J, Lv R, Peng H, Fan J, Liu Y (2020) Phosphate functionalized poly(vinyl alcohol)/poly(acrylic acid) (PVA/PAA): an electrospinning nanofiber for uranium separation. J Radioanal Nucl Ch 326(1):475–486
37. Zulfikar MA, Maulina D, Nasir M, Handayani N, Handajani M (2020) Removal of methylene blue from aqueous solution using poly (acrylic acid)/SiO2 and functionalized poly (acrylic acid)/SiO2 composite nanofibers. Environ Nanotechnol Monitoring Manag 14:100381
38. Park JA, Kang JK, Lee SC, Kim SB (2017) Electrospun poly(acrylic acid)/poly(vinyl alcohol) nanofibrous adsorbents for Cu(II) removal from industrial plating wastewater. RSC Adv 7(29):18075–18084
39. Xiao SL, Luo XY, Peng QY, Deb H (2016) Effective removal of calcium ions from simulated hard water using electrospun polyelectrolyte nanofibrous mats. Fiber Polym 17(9):1428–1437
40. Zhang SJ, Shi QT, Christodoulatos C, Korfiatis G, Meng XG (2019) Adsorptive filtration of lead by electrospun PVA/PAA nanofiber membranes in a fixed-bed column. Chem Eng J 370:1262–1273
41. Kim J, Kang T, Kim H, Shin HJ, Oh S-G (2019) Preparation of PVA/PAA nanofibers containing thiol-modified silica particles by electrospinning as an eco-friendly Cu(II) adsorbent. J Ind Eng Chem 77:273–279
42. Xiao SL, Ma H, Shen MW, Wang SY, Huang QG, Shi XY (2011) Excellent copper(II) removal using zero-valent iron nanoparticle-immobilized hybrid electrospun polymer nanofibrous mats. Colloid Surface A 381(1–3):48–54
43. Song S, Yin L, Wang XX, Liu L, Huang SY, Zhang R, Wen T, Yu SJ, Fu D, Hayat T, Wang XK (2018) Interaction of U(VI) with ternary layered double hydroxides by combined batch experiments and spectroscopy study. Chem Eng J 338:579–590
44. Wang PY, Yin L, Wang XX, Zhao GX, Yu SJ, Song G, Xie J, Alsaedi A, Hayat T, Wang XK (2018) L-cysteine intercalated layered double hydroxide for highly efficient capture of U(VI) from aqueous solutions. J Environ Manage 217:468–477
45. Karami Z, Jouyandeh M, Ali JA, Ganjali MR, Aghazadeh M, Maadani M, Saeb MR (2019) Development of Mg-Zn-Al-CO_3 ternary LDH and its curability in epoxy/amine system. Prog Org Coat 136:105264
46. Zou YD, Wang XX, Wu F, Yu SJ, Hu YZ, Song WC, Liu YH, Wang HQ, Hayat T, Wang XK (2017) Controllable synthesis of Ca-Mg-Al layered double hydroxides and calcined layered double oxides for the efficient removal of U(VI) from wastewater solutions. ACS Sustain Chem Eng 5(1):1173–1185
47. Butenko E, Bish D, Abrosimova G, Kapustin A (2013) Comparison of sorption properties of natural and synthetic takovites, $Ni_6Al_2(OH)_{16}CO_3{\cdot}4H_2O$. Építőanyag: JSBCM 65(4):97–101
48. Valeikiene L, Roshchina M, Grigoraviciute-Puroniene I, Prozorovich V, Zarkov A, Ivanets A, Kareiva A (2020) On the Reconstruction Peculiarities of Sol-Gel Derived $Mg_{2-x}M_x/Al_1$(M = Ca, Sr, Ba) Layered Double Hydroxides. Curr Comput-Aided Drug Des 10(6):470
49. Li Y, He H, Liu Z, Lai Z, Wang Y (2021) A facile method for preparing three-dimensional graphene nanoribbons aerogel for uranium (VI) and thorium (IV) adsorption. J Radioanal Nuclear Chem 328(1):289–298
50. Aslani CK, Amik O (2021) Active Carbon/PAN composite adsorbent for uranium removal: Modeling adsorption isotherm data, thermodynamic and kinetic studies. Appl Radiation and Isotopes 168:109474
51. Hu R, Xiao J, Wang T, Chen G, Chen L, Tian X (2020) Engineering of phosphate-functionalized biochars with highly developed surface area and porosity for efficient and selective extraction of uranium. Chem Eng J 379:122388
52. Li P, Chen P, Liu Z, Nie S, Wang X, Wang G, Wang L (2020) Highly efficient elimination of uranium from wastewater with facilely synthesized Mg-Fe layered double hydroxides: Optimum preparation conditions and adsorption kinetics. Anna Nuclear Energy 140:107140
53. Huang Y, Zheng H, Li H, Zhao C, Zhao R, Li S (2020) Highly selective uranium adsorption on 2-phosphonobutane-1, 2, 4-tricarboxylic acid-decorated chitosan-coated magnetic silica nanoparticles. Chem Eng J 388:124349
54. Liu L, Lin XY, Li MS, Chu HH, Wang HY, Xie Y, Du ZC, Liu MJ, Liang LL, Gong HY, Zhou J, Li ZG, Luo XG (2021) Microwave-assisted hydrothermal synthesis of carbon doped with phosphorus for uranium(VI) adsorption. J Radioanal Nucl Ch 327(1):73–89
55. Wang Y, Li YX, Li L, Kong FG, Lin S, Wang ZQ, Li WL (2020) Preparation of three-dimensional fiber-network chitosan films for the efficient treatment of uranium-contaminated effluents. Water Sci Technol 81(1):52–61
56. Yang S, Li Q, Chen L, Chen Z, Hu B, Wang H, Wang X (2020) Synergistic removal and reduction of U (VI) and Cr (VI) by Fe3S4 micro-crystal. Chem Eng J 385:123909
57. Alahabadi A, Singh P, Raizada P, Anastopoulos I, Sivamani S, Dotto GL, Hosseini-Bandegharaei A (2020) Activated carbon from wood wastes for the removal of uranium and thorium ions through modification with mineral acid. Colloids Surf A Physicochem Eng Aspects 607:125516